AGU PUBLICATIONS

JGR

Journal of Geophysical Research: Solid Earth

RESEARCH ARTICLE
10.1002/2015JB012701

Key Points:
- Hexagonal Fe_7C_3 exhibits elastic softening between 7 GPa and 20 GPa at 300 K
- Noncollinear alignment of Fe spin can explain the elastic softening in Fe_7C_3
- The elastic softening enhances the stability of Fe_7C_3 in the Earth's mantle

Supporting Information:
- Table S1

Correspondence to:
J. Liu,
jiacliu@umich.edu

Citation:
Liu, J., J. Li, and D. Ikuta (2016), Elastic softening in Fe_7C_3 with implications for Earth's deep carbon reservoirs, *J. Geophys. Res. Solid Earth*, *121*, 1514–1524, doi:10.1002/2015JB012701.

Received 30 NOV 2015
Accepted 21 FEB 2016
Accepted article online 26 FEB 2016
Published online 12 MAR 2016

Elastic softening in Fe_7C_3 with implications for Earth's deep carbon reservoirs

Jiachao Liu[1], Jie Li[1], and Daijo Ikuta[2]

[1]Department of Earth and Environmental Sciences, University of Michigan, Ann Arbor, Michigan, USA, [2]High Pressure Collaborative Access Team, Geophysical Laboratory, Carnegie Institution of Washington, Argonne, Illinois, USA

Abstract Iron carbide Fe_7C_3 has recently emerged as a potential host of reduced carbon in Earth's mantle and a candidate component of the inner core, but the equation of state of Fe_7C_3 is still uncertain, partly because the nature of pressure-induced magnetic transitions in Fe_7C_3 and their elastic effects remain controversial. Here we report the compression curve of hexagonal Fe_7C_3 in neon medium with dense pressure sampling and in comparison with pure iron in the same loading. The results revealed elastic softening between 7 GPa and 20 GPa, which can be attributed to noncollinear alignment of spin moments in a state between the ferromagnetic and paramagnetic phases, as expected for Invar-type alloys. The volume reduction associated with the softening would enhance the stability of Fe_7C_3 in the deeper part of the upper mantle and transition zone. As a result of subsequent spin crossover at higher pressures, Fe_7C_3 at inner core conditions likely occurs as the nonmagnetic phase, which remains a candidate for the major component of the Earth's central sphere.

1. Introduction

Carbon is considered a candidate light element in the Earth's core because it is the fourth most abundant element in the solar system and has strong affinity for both solid and liquid iron [*Wood*, 1993]. Experimental studies on the Fe-C binary system suggest that at high pressures Fe_7C_3 occurs as the liquidus phase if the carbon content exceeds the eutectic value and that the eutectic composition may contain less than 1 wt % carbon [*Lord et al.*, 2009]. On the other hand, there may be as much as 1 wt % carbon in the Earth's core [*Dasgupta and Walker*, 2008; *Nakajima et al.*, 2009; *Wood et al.*, 2013; *Dasgupta et al.*, 2013], and therefore its solidification could have produced Fe_7C_3 as the dominant phase of the inner core. The hypothesis of a carbon-rich inner core has gained support because Fe_7C_3 appears to provide a good match for the density of the inner core [*Nakajima et al.*, 2011; *Chen et al.*, 2012] and can explain its anomalously low shear wave velocity [*Chen et al.*, 2014] and high Poisson's ratio [*Prescher et al.*, 2015]. There are, however, significant discrepancies in the reported pressures of magnetic transitions in Fe_7C_3 and the associated effects on its elasticity [*Nakajima et al.*, 2011; *Mookherjee et al.*, 2011; *Chen et al.*, 2012; *Prescher et al.*, 2015], thus introducing uncertainties in estimating its density at core conditions.

At ambient conditions, Fe_7C_3 occurs in structures that belong to two crystal systems: A hexagonal polytype (h-Fe_7C_3) with the space group $P6_3mc$, known as the Eckstrom-Adcock carbide, and orthorhombic polytypes (o-Fe_7C_3) with possible space groups *Pnma*, *Pmcn*, and *Pbca* [*Eckstrom and Adcock*, 1950; *Herbstein and Snyman*, 1964; *Fruchart and Rouault*, 1969; *Tsuzuki et al.*, 1984; *Litasov et al.*, 2015; *Prescher et al.*, 2015]. Both the hexagonal and orthorhombic structures have been observed at high pressures [*Nakajima et al.*, 2011; *Chen et al.*, 2012; *Prescher et al.*, 2015], but their relative stabilities are still under debate [*Xie et al.*, 2005; *Fang et al.*, 2009; *Raza et al.*, 2015].

Fe_7C_3 is ferromagnetic (fm) at 1 bar, and the Curie temperature (Tc) of the h-Fe_7C_3 is 523 K [*Tsuzuki et al.*, 1984]. Theoretical calculations on h-Fe_7C_3 predicted that the magnetic moments of the Fe atoms decrease with pressure, leading to fm to nonmagnetic (nm) transition near 67 GPa and at 0 K [*Mookherjee et al.*, 2011]. *Nakajima et al.* [2011] observed elastic stiffening at about 18 GPa in the compression curve of h-Fe_7C_3 at 300 K and interpreted it as a result of fm to paramagnetic (pm) transition. *Chen et al.* [2012, 2014] inferred fm to pm transition between 5.5 and 10 GPa on the basis of the disappearance of fast oscillation in the time domain Mössbauer spectrum. They also detected the pm to nm transition at 53 GPa as indicated by loss of magnetic moment on Fe atoms according to X-ray emission spectroscopy measurements. Furthermore, *Chen et al.* [2012, 2014] carried out X-ray diffraction and nuclear-resonant inelastic scattering measurements. They found elastic stiffening upon the fm to pm transition and softening resulting from

the pm to nm transition. Using energy domain Mössbauer spectroscopy and X-ray diffraction methods, *Prescher et al*. [2015] studied *o*-Fe_7C_3 and reported fm to pm transition near 16 GPa and pm to nm transition near 70 GPa, with no resolvable anomalies in its compression curve. A recent theoretical study of *o*-Fe_7C_3 at 0 K reported fm to nm transition at 80 GPa or 120 GPa depending on the calculation methods [*Raza et al*., 2015].

Fe_7C_3 belongs to a peculiar type of material known as Invar alloy, which is characterized by anomalously small thermal expansion below the Curie temperature [*Litasov et al*., 2015]. A prevailing theory known as the 2-γ state model explains the unusual behavior by thermally enhanced population of the smaller low-spin state at higher energy at the expense of the larger high-spin state at lower energy, which leads to volume reduction against thermal expansion [*Weiss*, 1963; *Nataf et al*., 2006]. Because the 2-γ state model failed to predict a number of experimental observations, *van Schilfgaarde et al*. [1999] postulated the occurrence of a noncollinear state, where the spin orientations of nearest-neighbor Fe-Fe pairs may be parallel as in the ferromagnetic state, antiparallel as in the antiferromagnetic state, or at a random angle as in the paramagnetic state, while other spin pairs maintain parallel alignments as expected for the ferromagnetic state. In the noncollinear model, thermal relaxation in spin alignment leads to volume reduction to compensate for thermal expansion. The noncollinear model provides explanations for experimentally observed responses of Fe-Ni Invar alloys to variations in concentration or pressure. Note that the two models are not mutually exclusive: The noncollinear model introduces freedom in spin alignment in addition to reduction of local magnetic moment, which applies in both models.

When typical Fe-Ni and Fe-Pt Invar alloys lose magnetic ordering upon compression, the effect manifests as anomalous softening [e.g., *Dubrovinsky et al*., 2001; *Nataf et al*., 2006; *Winterrose et al*., 2009]. Mössbauer measurements suggest that *h*-Fe_7C_3 and *o*-Fe_7C_3 undergo magnetic collapse near 7 and 16 GPa, respectively, yet elastic softening has not been reported to accompany these transitions [*Chen et al*., 2012, 2014; *Prescher et al*., 2015]. In an attempt to elucidate the nature of the fm to pm transition and its influence on elasticity, we investigated the compression behavior of *h*-Fe_7C_3 at 300 K with dense data coverage in the pressure range across the fm to pm transition. Furthermore, we included pure Fe in the same loading as a reference sample to monitor the effect of nonhydrostatic stress and used multiple pressure markers to measure pressure gradient and quantify uncertainties in pressure determination.

2. Experimental Methods

A polycrystalline Fe_7C_3 sample was synthesized from a mixture of fine iron and graphite powders at 14 GPa and 1473 K for 7 h using the multianvil apparatus at the University of Michigan. The starting material contained excess graphite relative to the stoichiometric composition to ensure that Fe_7C_3 was the only iron carbide in the run product. According to electron probe analysis, the composition of the run product $Fe_{6.95(11)}C_{3.05(11)}$ is stoichiometric within uncertainties. Its X-ray diffraction (XRD) pattern matches the hexagonal Fe_7C_3 with an ambient condition unit cell volume of 186.1(1) $Å^3$ (Table 1).

High pressures were generated using symmetric type diamond anvil cell (DAC) with 300 μm culet diamonds. A rhenium gasket, initially 250 μm thick, was preindented to about 27 GPa with the thickness thinned to 40 μm. A hole of 150 μm was drilled in the gasket and loaded with a piece of polycrystalline Fe_7C_3 aggregate that is approximately $30 \times 20 \times 7\ \mu m^3$, a flake of Fe of similar size, and two 10 μm ruby spheres and a $15 \times 15 \times 5\ \mu m^3$ sized Au flake as supplementary pressure standards (Figure 1). In addition, submicron-sized Au powder was spread on top of the Fe_7C_3 and Fe samples to serve as the primary pressure standard. Neon was loaded into the sample chamber as a hydrostatic pressure medium and an additional pressure standard by using the COMPRES/GSECARS gas-loading system at the Advanced Photon Source (APS), Argonne National Laboratory.

Angle-dispersive XRD measurements were performed at beamline 16-BM-D of the Advanced Photon Source (APS). The incident X-ray beam has a monochromatic wavelength of 0.4246 Å and a full width at half maximum of 5 μm × 15 μm. Diffracted X-rays were recorded on a MAR345 image plate. The sample-to-detector distance and the tilt angle and rotation angle of the image plate relative to the incident X-ray beam were calibrated by 1 bar diffraction of cerium dioxide (CeO_2). At each pressure point the X-ray diffraction images of Fe_7C_3, Fe, and Au were recorded for an exposure time of 30 to 60 s. Data were collected at an interval of about 0.5 GPa for pressures below 10 GPa, 1 to 2 GPa between 10 and 20 GPa, and 2 to 4 GPa above 20 GPa. Ruby

Table 1. Equation of State Parameters of Fe_7C_3 and Iron at 300 K[a]

	P (GPa)	V_0 (Å^3)	K_0 (GPa)	K_0'
h-Fe_7C_3				
This study				
Ferromagnetic	0–7	186.1 (1)[b]	186 (5)	6.9 (2.2)
Noncollinear	7–20	186.9 (4)	166 (13)	4.9 (1.1)
Paramagnetic	20–66	184.6 (5)	196 (9)	4.9 (2)
Nakajima et al. [2011]				
Ferromagnetic	0–18	186.4 (1)	201 (2)	4 (fixed)
Paramagnetic	18–71.5	184.2 (3)	253 (7)	3.6 (2)
Chen et al. [2012]				
Paramagnetic	7–53	184.7 (2)	201 (12)	8.0 (1.4)
Nonmagnetic	53–167	182.9 (4)	307 (6)	3.2 (1)
o-Fe_7C_3				
Prescher et al. [2015]	4–158	186.2 (1)[c]	168 (4)	6.1 (1)
α-Fe				
This study	0–14.1	23.575 (2)[b]	157 (1)	4.8 (3)
Guinan and Beshers [1968] and *Robie et al.* [1978]	0–1	23.55 (1)	166 (2)	5.3 (3)

[a]Numbers in parentheses are uncertainties on the last digits.
[b]Measured value.
[c]Normalized to two formulas per unit cell.

fluorescence spectra were collected using the online system. The XRD images were integrated using the software Fit2D. Diffraction patterns were analyzed using the software FullProf to examine the crystal structure and extract lattice parameters.

3. Results

Two-dimensional X-ray diffraction images were recorded between 1 bar and 66 GPa and at 300 K (Figure 2) and integrated into one-dimensional patterns (Figure 3). At 1 bar the XRD pattern is consistent with that of *h*-Fe_7C_3 [*Herbstein and Snyman*, 1964] and does not match those of *o*-Fe_7C_3 because at least 10 expected peaks are missing (Figure 3b). At 1.5 GPa, one peak at 11.01° or 2.213 Å with asymmetric shape does not belong to the *h*-Fe_7C_3 pattern but matches the (201) peak of *o*-Fe_7C_3 with the space group *Pnma* (Figure 3 b). The peak was also observed in previous studies on *h*-Fe_7C_3 [*Herbstein and Snyman*, 1964; *Nakajima et al.*, 2011]. In this study it shifted with pressure at a similar rate as other *h*-Fe_7C_3 peaks and persisted to the highest pressure. Another peak at 11.3° or 2.155 Å is likely the (200) peak of FeO impurity, as seen in electron probe analysis. The presence of these two peaks does not affect the derived lattice parameters because they have relatively low intensities and do not overlap with other peaks. The lattice parameters of *h*-Fe_7C_3

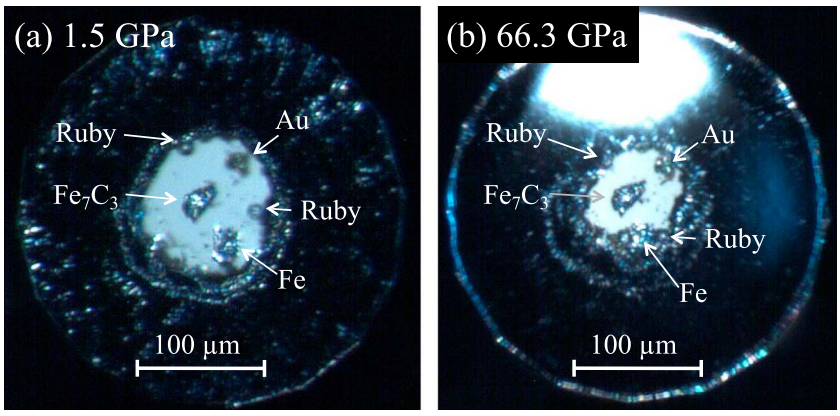

Figure 1. Optical images showing the sample configuration. (a) At 1.5 GPa and (b) at 66.3 GPa. The sample chamber contains Fe_7C_3 in the center, Au at the upper right corner, Fe near the bottom, and ruby balls near the top, on the right, or near the lower right corner. Au powder was spread on top of the Fe_7C_3 and Fe samples.

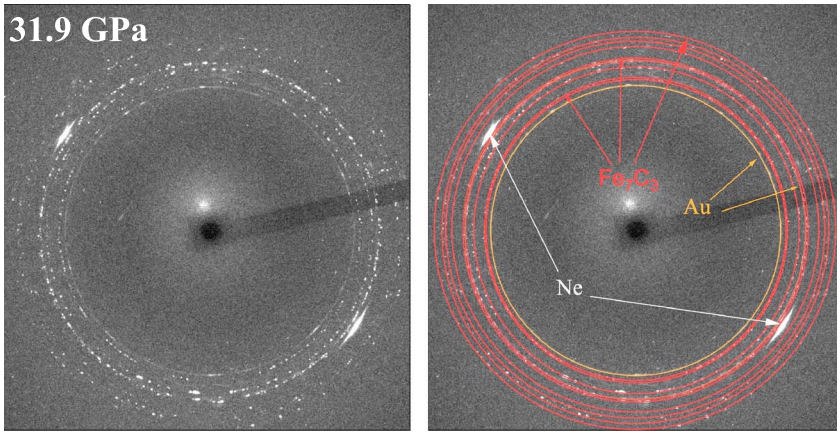

Figure 2. Representative X-ray diffraction image of *h*-Fe_7C_3 at 31.9 GPa (wavelength = 0.4246 Å). The Debye-Scherrer rings of Fe_7C_3 (marked red on the right) and Au (gold) are nearly continuous whereas that of Ne (white arrows) appear as two arcs.

were fitted from 8 to 11 diffraction peaks including (201), (120), (002), (012), (121), (300), (112), (301), (202), (220), and (212). The lattice parameter of α-Fe was determined from the (110) peak, and those of ε-Fe were determined from the (100), (002), and (101) peaks.

The compression data at 300 K revealed that *h*-Fe_7C_3 became more compressible or softens between about 7 and 20 GPa (Figure 4a). For comparison, the compression curves of α-Fe and ε-Fe in the same sample chamber confirmed the known phase transition near 14 GPa and remained smooth otherwise (Figures 4a–4b). The changes in the compression behavior manifest as three distinct segments in the normalized pressure $F = P/3f(1+2f)^{5/2}$ versus Eulerian strain $f = [(V/V_0)^{-2/3}-1]/2$ plot, with a short segment of positive slope at low pressures, followed by a segment of negative slope between 4 to 7 GPa and 16 to 20 GPa, and then another long segment of positive slope at high pressures (Figure 4c). The BM-EOS fits to the three segments show that near 7 GPa the bulk modulus of *h*-Fe_7C_3 decreases indicating softening, and then near 20 GPa the bulk modulus increases indicating stiffening (Table 1, Figure 4a). An obvious change in slope near 20 GPa is also seen in the *a*/*c* ratio versus pressure plot of *h*-Fe_7C_3, whereas the *F*-*f* and axial ratio plots of Fe show no change in pure Fe except near the α and ε-Fe phase boundary (Figure 4).

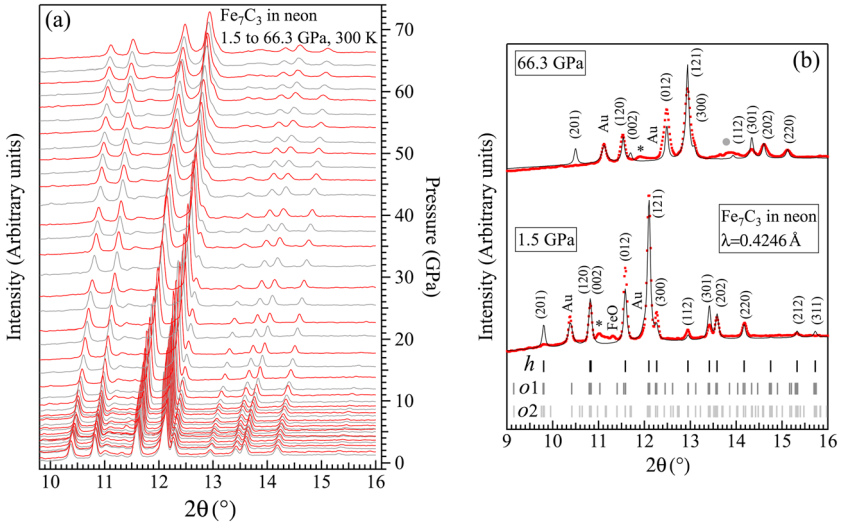

Figure 3. X-ray diffraction patterns of *h*-Fe_7C_3 at 300 K. (a) Stacked patterns between 1.5 GPa and 66.3 GPa, vertically shifted in proportion to pressure. (b) Measured patterns (red) with Rietveld fittings (black) at 1.5 GPa and 66.3 GPa, marked with *h*-Fe_7C_3 peaks with Miller indices, Au and FeO peaks, an unknown peak (asterisk), along with the expected peak positions of *h*-Fe_7C_3 with $P6_3mc$ space group (black ticks) and *o*-Fe_7C_3 with the space groups *Pnma* (dark gray ticks labeled as *O*1) and *Pbca* (light gray ticks labeled as *O*2) at 1.5 GPa. A neon peak (gray dot) is masked out because it overlaps with the (112) peak of Fe_7C_3.

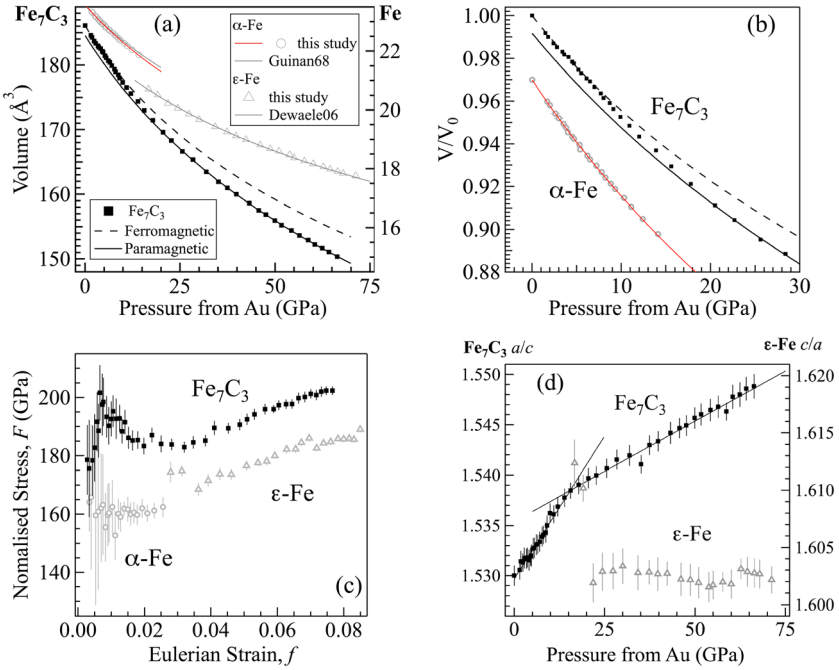

Figure 4. Compression behavior of *h*-Fe_7C_3 and Fe at 300 K and up to 71 GPa. (a) Unit cell volume of *h*-Fe_7C_3 (solid squares) and third-order Birch-Murnaghan equations of state (BM-EOS) fits to the data between 1 bar and 7 GPa (black dashed) and between 20 GPa and 66 GPa (black solid). Unit cell volume of α-Fe (gray open circles) and ε-Fe (gray open triangles) in the same diamond anvil cell, together with a third-order BM-EOS fit to the data between 1 bar and 7 GPa (red solid) and existing compression curves of α-Fe (gray solid, *Guinan and Beshers* [1968]) and ε-Fe (gray solid, *Dewaele et al*. [2006]). The fitting of a third-order BM-EOS to the α-Fe data between 1 bar and 7 GPa (red solid) passes through the data at higher pressures, indicating smooth compression. (b) Normalized volumes of Fe_7C_3 (solid squares) and α-Fe (open circles) up to 30 GPa. The third-order BM-EOS fits to the *h*-Fe_7C_3 data reveal softening in *h*-Fe_7C_3 between 7 and 20 GPa. (c) Finite Eulerian strain *F* versus normalized stress *f* for *h*-Fe_7C_3, α-Fe, and ε-Fe, revealing two discontinuities for Fe_7C_3 at 4 to 7 GPa and 16 to 20 GPa, respectively, and confirming the discontinuity associated with the α-Fe to ε-Fe transition [*Dewaele et al*., 2006]. (d) Axial ratios of *h*-Fe_7C_3 and ε-Fe up to 71 GPa at 300 K, revealing a kink near 20 GPa for *h*-Fe_7C_3 and confirming the expected discontinuity associated with the α-ε phase boundary of Fe [*Wang and Ingalls*, 1998]. The uncertainties are represented by the error bars or smaller than the sizes of symbols. Data are listed in Table S1.

4. Discussion

4.1. Nature of Magnetic Transitions in *h*-Fe_7C_3

The observed elastic softening between 7 and 20 GPa is reminiscent of the compression behavior of Invar alloys [*Dubrovinsky et al*., 2001; *Nataf et al*., 2006; *Winterrose et al*., 2009] but may also result from a gradual spin-pairing transition in iron [e.g., *Crowhurst et al*., 2008; *Chen et al*., 2014]. Here the smooth compression on pure iron in the same loading indicates that the observed softening did not result from artifacts such as nonhydrostatic pressure. Moreover, the compression curves of iron from this study reproduced existing data using helium pressure medium [*Dewaele et al*., 2006], thus confirming close approach to hydrostaticity in the experiments. Between 1 bar and 25 GPa, the good match in pressures determined from gold marker placed on top of the sample and that of neon marker surrounding the sample further supports that the sample environment is nearly hydrostatic.

Between 1 bar and about 20 GPa, the data from previous studies are in general agreement with this study (Figure 5). The softening observed here, however, has not been reported in previous studies: *Nakajima et al*. [2011] measured the compression curves of *h*-Fe_7C_3 and observed stiffening near 18 GPa at 300 K; *Chen et al*. [2012] fitted an equation of state (EoS) to the data between 7 and 53 GPa and by comparison to *Nakajima et al*. [2011] results inferred stiffening near 7 GPa; *Prescher et al*. [2015] studied *o*-Fe_7C_3 and detected stiffening in the mean Fe-C distance near 16 GPa. We interpret the reported stiffening at 16 or 18 GPa as a manifestation of the elastic softening between 7 and 20 GPa and attribute the discrepancies to sparse data coverage in the

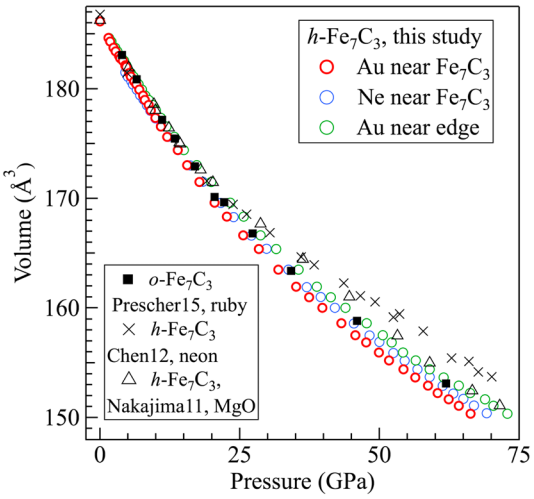

Figure 5. Compression curves of Fe_7C_3 from different studies. In this study, the pressure in the diamond cell varied by as much as 7 GPa at 66 GPa according to multiple markers, including ruby [*Mao et al.* [1986]], Au near the sample (red circles, *Fei et al.* [2007]), Ne near the sample (blue circles, *Dewaele et al.* [2008]), and Au near the edge of the sample chamber (green circles). The discrepancies among this study, *Prescher et al.* [2015] (square), *Chen et al.* [2012] (cross), and *Nakajima et al.* [2011] (open triangle) may in part arise from pressure gradient.

low-pressure range: Between 1 bar and 20 GPa, *Nakajima et al.* [2011] collected six data points in one experiment and eight in another, whereas *Chen et al.* [2012] and *Prescher et al.* [2015] each collected six data points. Lumping the data between 1 bar and 20 GPa together, the softening below 20 GPa would appear as stiffening near 20 GPa. In this study, 26 data points were collected in a single experiment between 1 bar and 20 GPa, thus allowing us to resolve the softening between 7 and 20 GPa.

The classical $Fe_{0.64}Ni_{0.36}$ Invar alloy exhibits subtle softening between 2 and 6 GPa, before transforming to the pm phase [*Moruzzi*, 1990; *Dubrovinsky et al.*, 2001; *Nataf et al.*, 2006]. Although the effect was reported earlier as hardening near the end of the transition because of sparse data coverage [*Oomi and Mori*, 1981], at higher nickel content, $Fe_{0.55}Ni_{0.45}$ and $Fe_{0.20}Ni_{0.80}$ show clear softening between 9 and 14 GPa and between 5 and 9 GPa, respectively [*Dubrovinsky et al.*, 2001]. More pronounced softening with 3 to 4% volume reduction was observed in $Fe_{72}Pt_{28}$ [*Nataf et al.*, 2006] and Pd_3Fe [*Winterrose et al.*, 2009] Invar alloys. The subtle nature of softening in the Fe-Ni alloys was explained by the itinerant character of their magnetic properties [*Nataf et al.*, 2006]. The compressional softening shares the same origin as the Invar behavior, which refers to anomalously low thermal expansions. The magnetovolumic effect during heating or compression may be attributed to the rising population of the low-spin state with smaller volume, known as the 2-γ state model [e.g., *Weiss*, 1963; *Nataf et al.*, 2006]. Alternatively, the effect may be associated with a gradual transition from the fm state at larger volume to a disordered noncollinear configuration at smaller volumes [*van Schilfgaarde et al.*, 1999].

The 2-γ state model predicts that as Fe_7C_3 transforms from the fm to pm state, the local spin moments of some iron atoms are reduced but the iron spins are aligned in parallel and remain ferromagnetically ordered. According to the noncollinear model, the transition from the fm state to pm state is associated with increasing disorder in the alignment of iron spins and likely results in more rapid reduction in the magnetic moment of the bulk sample than the reduction in the spin magnetic moment of individual atoms [*van Schilfgaarde et al.*, 1999]. The X-ray emission and Mössbauer data [*Chen et al.*, 2012, 2014] showed that the local spin magnetic moment of iron atoms in *h*-Fe_7C_3 was constant between 1 bar and about 7 GPa and only began to decrease after the fast oscillation signal in the Mössbauer spectrum disappeared near 7 GPa. The disappearance of fast oscillation indicates loss of magnetic order, which may result from strong reduction in overall magnetic moment or from broadening of magnetic sextet peaks due to a less ordered state. The behavior of Fe_7C_3 thus favors the noncollinear theory, which predicts more rapid reduction in overall magnetic moment than local spin. At 20 GPa, iron atoms in *h*-Fe_7C_3 still possessed finite spin [*Chen et al.*, 2014], suggesting that the elastic softening in *h*-Fe_7C_3 between 7 and 20 GPa likely corresponds to a noncollinear state during a broad transition from the fm to pm state, instead of spin transition. This interpretation implies that the Curie temperature of *h*-Fe_7C_3 drops from 523 K at 1 bar to 300 K at about 20 GPa, at an average rate of −10 K/GPa. The rate is consistent with that of *Nakajima et al.* [2011], where a negative pressure-temperature (*P-T*) slope of the fm to pm transition was inferred from the elastic anomaly at 18 GPa and 300 K and its absence at temperatures above 500 K. A similar transition seems to occur in *o*-Fe_7C_3 where stiffening in the mean Fe-C distance and disappearance of magnetic sextet were detected near 16 GPa [*Prescher et al.*, 2015].

Spin-pairing transition is characterized by spin reduction alone and may coincide with the collapse of magnetic order if the material transforms directly from the fm state with finite spin to the nonmagnetic state

with zero spin, without going through the pm state with finite spin. In *h*-Fe_7C_3, pressure-induced collapse of magnetic order preceded spin-pairing transition, as discussed earlier. X-ray emission data showed that the local spin moment of Fe dropped to zero at 53 GPa, indicating the end of a broad spin-pairing transition [*Chen et al*., 2014]. The transition was associated with reductions in the shear and bulk modulus in *h*-Fe_7C_3 [*Chen et al*., 2012, 2014] and an increase in the Poisson's ratio in *o*-Fe_7C_3 [*Prescher et al*., 2015]. The observed transition pressure to the nm state is close to the calculated value of 67 GPa, even though the theoretical prediction applies to a transition from the magnetically ordered fm state instead of the magnetically disordered pm state [*Mookherjee et al*., 2011]. Moreover, experiments showed elastic softening instead of the predicted stiffening [*Mookherjee et al*., 2011; *Chen et al*., 2012]. The pm-nm transition was not detected in this study due to the limited pressure coverage. Despite discrepancies in details, existing studies agree upon a spin-pairing transition between 50 and 70 GPa accompanied by changes in elasticity.

For comparison, the fm to pm transition in Fe_3C was detected at 4 to 6 GPa from synchrotron Mössbauer spectroscopy measurements [*Gao et al*., 2008], magnetic susceptibility study [*Walker et al*., 2015], and X-ray diffraction measurements [*Litasov et al*., 2013], or at 8 to 10 GPa on the basis of the X-ray magnetic circular dichroism study [*Duman et al*., 2005] and conventional Mössbauer spectroscopy measurements [*Prescher et al*., 2012]. Even though most studies reported stiffening near the fm to pm transition pressure, softening is visible from some of the powder and single-crystal X-ray diffraction data [*Prescher et al*., 2012; *Litasov et al*., 2013]. Pressure-induced transition to the nm state has been reported for Fe_3C as well, but the transition pressure ranges between 22 GPa and 60 GPa [*Vocadlo et al*., 2002; *Lin et al*., 2004; *Ono and Mibe*, 2010; *Prescher et al*., 2012].

Some of the discrepancies in the pressures of magnetic transitions in Fe_7C_3 or Fe_3C may be associated with stress condition, sample composition, and data coverage. Magnetic transitions are known to be sensitive to nonhydrostatic stress because of magnetoelastic coupling effect. For instance, at 300 K mechanically stressed $Fe_{64}Ni_{36}$ Invar alloy loses its magnetic order near 10 GPa, whereas unstressed sample becomes paramagnetic near 6 GPa [*Gorria et al*., 2009]. Moreover, deviation from stoichiometry in Fe_3C was found to affect the pressure of magnetic transitions by 1 to 2 GPa [*Walker et al*., 2015]. Finally, a transition may be missed or misplaced as a result of sparse data coverage or sensitivities of the methods in detecting various types of transitions.

4.2. Magnetic EoS of *h*-Fe_7C_3

On the basis of the above discussion, we fit four equations of state to the compression curve of *h*-Fe_7C_3, for the fm phase between 1 bar and 7 GPa, the noncollinear state between 7 and 20 GPa, the pm phase from 20 to 60 GPa, and the nm phase above 60 GPa (Table 1). We choose 7 GPa as the low-pressure boundary of the noncollinear phase because the Mössbauer measurements detected magnetic collapse between 7.1 and 7.5 GPa [*Chen et al*., 2014]. The choice of 20 GPa as the high-pressure boundary of the noncollinear phase is somewhat arbitrary. The fitted EoS parameters of the fm and pm phases from this study differ from some of the previous results, partly because of uncertainties in the pressures of magnetic transitions, as discussed earlier. For example, *Chen et al*. [2012] interpreted the disappearance of fast oscillation in Mössbauer spectra between 5.5 and 7.5 GPa as the end of a magnetic-ordering transition. Accordingly, they fitted a pm-EoS to the data between 7 and 53 GPa and reported an unusually large K' of 8. Furthermore, nonstoichiometry in Fe_7C_3 may generate dislocations and defects and affect the elastic behavior [*Walker et al*., 2013, 2015].

Discrepancies in the fitted EoS parameters may also arise from differences among pressure markers and the presence of pressure gradient in the sample chamber (Figure 5). *Chen et al*. [2014] used single crystals in neon medium and laser annealed the samples up to 1200 K. They used neon and ruby as pressure standards in two experiments between 1 bar and 75 GPa and neon and Au as pressure standards in another experiment between 26 and 167 GPa. Their data are plotted against neon pressure. In *Nakajima et al*. [2011], the multi-anvil experiments used a mixture of Fe_7C_3 and MgO as the sample and MgO and Au as pressure standards. Data at 300 K and high temperature were collected up to 25 GPa. The DAC experiments used pelletized samples in MgO pressure medium and laser annealed the samples. They used MgO as the pressure standard. Data were collected at 300 K between 30 and 70 GPa. Their data were plotted against MgO pressure. *Prescher et al*. [2015] used ruby to measure pressure. In this study, the pressures from multiple markers or from the Au markers at different locations in the sample chamber diverged upon compression, with the discrepancy increasing from 1 or 2 GPa at 20 GPa to 3 to 7 GPa at 66 GPa (Table S1 in the supporting information). The presence of

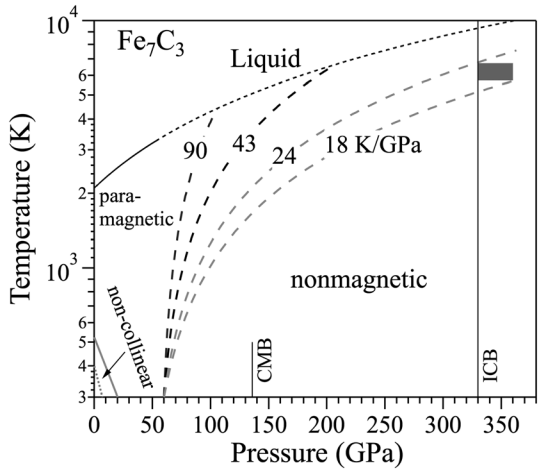

Figure 6. Schematic magnetic phase diagram of Fe_7C_3. The fm to noncollinear boundary (gray dotted line) at 300 K is placed at 7 GPa based on Mössbauer measurements [*Chen et al*., 2012, 2014] and anomaly in compression curve (this study), while this boundary at 1 bar is tentatively placed at about 400 K. The boundary between noncollinear and pm transition (gray solid line) is constrained by the Curie temperature of 523 K at 1 bar [*Tsuzuki et al*., 1984] and that of 300 K at 20 GPa (this study). The pm to nm transition or spin-pairing transition at 300 K is placed at 60 GPa by averaging the reported transition pressures [*Mookherjee et al*., 2011; *Chen et al*., 2012, 2014]. The black dashed curves represent the slopes of spin transition boundary of $(Mg,Fe)CO_3$ at about 90 K/GPa [*Liu et al*., 2014] and that of (Mg,Fe)O at about 43 K/GPa [*Mao et al*., 2012]. The melting curve (*Lord et al*. [2009], thin black lines) with linear extrapolation to higher pressures as dotted curve through CMB (core-mantle boundary) and ICB (inner core boundary). At the estimated range of inner core temperature at 6230 ± 500 K (gray shaded box, *Anzellini et al*. [2013]), if the slope of spin transition boundary exceeds 24 K/GPa, only nonmagnetic Fe_7C_3 is stable at the inner core's *P-T* conditions. If the slope falls between 18 and 24 K/GPa (gray dashed lines), both the paramagnetic and nonmagnetic Fe_7C_3 are stable. For smaller slopes, only the paramagnetic Fe_7C_3 is stable.

pressure gradients in the sample chambers or the choice of pressure markers alone seems sufficient to account for the inconsistencies between various EoS.

4.3. Fe_7C_3 in Earth's Mantle and Inner Core

A number of studies suggested that metallic iron might be present at depths greater than about 250 km in the mantle where ferric ion Fe^{3+} becomes stabilized in pyroxene, garnet, or bridgmanite [e.g., *Frost et al*., 2004; *Rohrbach et al*., 2007; *Stagno et al*., 2013]. The metallic iron could react with subducted carbonates to produce elemental carbon or iron carbides [e.g., *Rohrbach and Schmidt*, 2011]. The relative stabilities of potential host phases for reduced carbon in the mantle, including diamond, Fe_3C, Fe_7C_3, and other Fe-C alloys, is unknown. In the iron-carbon binary system, Fe_7C_3 is not stable at pressures below 5 GPa and it forms at 5 to 7 GPa through subsolidus reaction between Fe_3C and diamond or graphite [*Tsuzuki et al*., 1984; *Fei and Brosh*, 2014]. In this study, the noncollinear state of Fe_7C_3 is found to be as much as 1% denser than the extrapolated values of the corresponding ferromagnetic state (Figure 4a). The volume reduction would lower the Gibbs energy of Fe_7C_3 and enhance its stability between 7 and 20 GPa, corresponding to 220 to 570 km depths range in Earth's mantle.

Considering that the bulk carbon content of the core is likely below about 1 wt %, having an Fe_7C_3-rich inner core requires that the core contains at least another lighter element in higher abundance that partitions strongly into the liquid to account for the density deficit in the outer core and that carbon strongly favors the solid during core crystallization. An additional critical test for the model of Fe_7C_3-dominant inner core is that the density of Fe_7C_3 under the relevant *P-T* conditions matches the observed values of 12.8–13.1 g/cc [*Dziewonski and Anderson*, 1981]. Because direct measurements are not yet available, current estimates rely on extrapolating the experimentally determined EoS to the inner core conditions. In order to assess the stable magnetic phase of Fe_7C_3 under the core's *P-T* conditions, we constructed a preliminary magnetic phase diagram (Figure 6). The temperature dependence of the spin-pairing transition pressure of Fe_7C_3 is unknown. Previous work found that the pressure of spin-pairing transition increased with temperature at the rate of 43 K/GPa for ferropericlase [*Mao et al*., 2012] or 90 K/GPa for magnesiosiderite [*Liu et al*., 2014]. If these values are applicable to *h*-Fe_7C_3, then it is expected to adopt the low-spin nm state under the inner core conditions with the estimated temperature of 6230 ± 500 K [*Anzellini et al*., 2013]. The pressure-temperature slope of the transition boundary for Fe_7C_3 may be smaller than oxides or carbonates. If the slope falls below 24 K/GPa but above 18 K/GPa, the pm-nm transition will happen in the inner core and a mixture of pm and nm phases would be stable under the relevant conditions. If the slope is smaller than 18 K/GPa, then the pm phase will be the only stable phase in the inner core.

Using the EoS parameters in Table 1 and the thermoelastic parameters reported in *Nakajima et al*. [2011], the densities of various Fe_7C_3 phases at inner core conditions are calculated (Figure 7). The temperature of the inner core is assumed to be 6230 ± 500 K, which is the melting point of pure iron, hence representing an

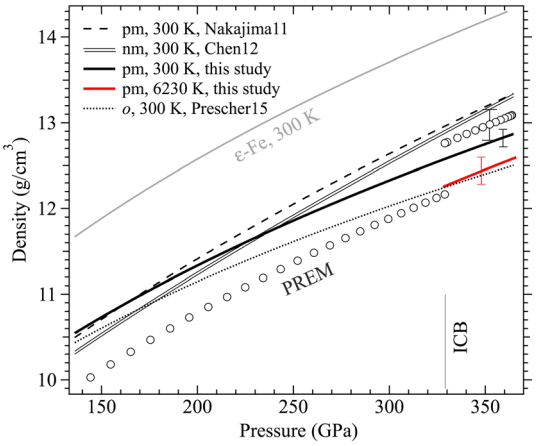

Figure 7. Estimated density profiles of Fe_7C_3 at core conditions compared with the PREM model (open circles with error bar, *Dziewonski and Anderson* [1981]). The calculated densities of *h*-Fe_7C_3 at the pressures of the inner core and 300 K from highest to lowest are paramagnetic phase of *Nakajima et al.* [2011] (dashed), nonmagnetic phase of *Chen et al.* [2012] (double line), paramagnetic phase of this study (black solid with error bar), and *o*-Fe_7C_3 of *Prescher et al.* [2015] (dotted). The density of ε-Fe at 300 K (thin gray curve, *Dewaele et al.* [2006]) is higher than PREM. Accounting for the thermal expansion effect [*Nakajima et al.*, 2011], the density of paramagnetic *h*-Fe_7C_3 at 6230 ± 500 K (red with error bar) is 4% lower than that of PREM, whereas that of the nonmagnetic *h*-Fe_7C_3 matches the PREM value [*Chen et al.*, 2012].

upper bound on the temperature at the inner core boundary [*Anzellini et al.*, 2013]. The densities of the pm *h*-Fe_7C_3 at the inner core conditions are about 4% lower than the Preliminary Reference Earth Model (PREM); therefore, the pm *h*-Fe_7C_3 is not a viable candidate for the dominant phase in the inner core. The nm *h*-Fe_7C_3, on the other hand, has been shown to provide a good match for the inner core density [*Chen et al.*, 2012]. Although the *h*-Fe_7C_3 and *o*-Fe_7C_3 have very similar densities up to 200 GPa, the extrapolated densities diverge and become 6% apart at inner core pressures. Because *o*-Fe_7C_3 at 300 K is already 4% lighter than PREM, it cannot match the density of the inner core. Considering the lack of direct experimental data at the relevant pressures and temperatures, further work is needed to provide tighter constraint on the densities of various polytypes of Fe_7C_3 at pressures above 2 Mbar and at high temperatures.

5. Conclusions

Using synchrotron X-ray diffraction and diamond anvil cell techniques, the compression behavior of a synthetic *h*-Fe_7C_3 has been investigated at 300 K and up to 66 GPa with dense data coverage, which allowed us to detect elastic softening between 7 and 20 GPa. The results were further corroborated by measurements on pure iron in the same loading, which eliminated experimental artifacts such as nonhydrostatic pressure as the cause of the observed softening. Instead, the softening can be explained by volume reduction associated with noncollinear spin alignment in a transitional state between the ferromagnetic and paramagnetic phases, as expected for Invar-type alloys. Accordingly, the compression behavior of *h*-Fe_7C_3 within the pressure range of the Earth's interior can be described by equations of state of four phases with distinct magnetic properties: The ferromagnetic phase between 1 bar and 7 GPa, the noncollinear phase between 7 and 20 GPa, the paramagnetic phase between 20 and about 60 GPa, and the nonmagnetic phase above 60 GPa. The elastic softening between 7 and 20 GPa implies enhanced stability of *h*-Fe_7C_3 in the deeper part of Earth's upper mantle and transition zone. Considering the temperature dependence of the spin-pairing transition pressure, *h*-Fe_7C_3 likely occurs as the nm phase and remains a viable candidate component for the inner core. Given the lack of direct experimental data at the relevant pressures and temperatures, further work is needed to resolve the controversies concerning the structure, stability, and physical properties of Fe_7C_3 at inner core conditions.

Acknowledgments

We thank two anonymous reviewers for providing encouraging, thoughtful, and constructive suggestions and Burkhard Militzer and Dave Walker for helpful discussion on magnetism. This research was partially supported by NSF AST 1344133 and EAR 1219891, NASA NNX10AG97G and NNX15AG54G, and Sloan Foundation Deep Carbon Observatory grant G-2015-14085. Portions of the work were performed at HPCAT (Sector 16), Advanced Photon Source (APS), Argonne National Laboratory. The data for this paper are available by contacting the corresponding author Jiachao Liu (jiacliu@umich.edu).

References

Anzellini, S., A. Dewaele, M. Mezouar, P. Loubeyre, and G. Morard (2013), Melting of iron at Earth's inner core boundary based on fast X-ray diffraction, *Science*, *340*(6131), 464–466.

Chen, B., L. L. Gao, B. Lavina, P. Dera, E. E. Alp, J. Y. Zhao, and J. Li (2012), Magneto-elastic coupling in compressed Fe_7C_3 supports carbon in Earth's inner core, *Geophys. Res. Lett.*, *39*, L18301, doi:10.1029/2012GL052875.

Chen, B., et al. (2014), Hidden carbon in Earth's inner core revealed by shear softening in dense Fe_7C_3, *Proc. Natl. Acad. Sci. U.S.A.*, *111*(50), 17,755–17,758.

Crowhurst, J. C., J. M. Brown, A. F. Goncharov, and S. D. Jacobsen (2008), Elasticity of (Mg,Fe)O through the spin transition of iron in the lower mantle, *Science*, *319*(5862), 451–453.

Dasgupta, R., and D. Walker (2008), Carbon solubility in core melts in a shallow magma ocean environment and distribution of carbon between the Earth's core and the mantle, *Geochim. Cosmochim. Acta*, *72*(18), 4627–4641.

Dasgupta, R., H. Chi, N. Shimizu, A. S. Buono, and D. Walker (2013), Carbon solution and partitioning between metallic and silicate melts in a shallow magma ocean: Implications for the origin and distribution of terrestrial carbon, *Geochim. Cosmochim. Acta*, *102*, 191–212.

Dewaele, A., P. Loubeyre, F. Occelli, M. Mezouar, P. I. Dorogokupets, and M. Torrent (2006), Quasihydrostatic equation of state of iron above 2 Mbar, *Phys. Rev. Lett.*, *97*(21), 215504.

Dewaele, A., F. Datchi, P. Loubeyre, and M. Mezouar (2008), High pressure-high temperature equations of state of neon and diamond, *Phys. Rev. B*, *77*(9), 094106.
Dubrovinsky, L., N. Dubrovinskaia, I. A. Abrikosov, M. Vennstrom, F. Westman, S. Carlson, M. van Schilfgaarde, and B. Johansson (2001), Pressure-induced invar effect in Fe-Ni alloys, *Phys. Rev. Lett.*, *86*(21), 4851–4854.
Duman, E., M. Acet, E. F. Wassermann, J. P. Itie, F. Baudelet, O. Mathon, and S. Pascarelli (2005), Magnetic instabilities in Fe_3C cementite particles observed with FeK-edge X-ray circular dichroism under pressure, *Phys. Rev. Lett.*, *94*(7), 075502.
Dziewonski, A. M., and D. L. Anderson (1981), Preliminary reference Earth model, *Phys. Earth Planet. Int.*, *25*(4), 297–356.
Eckstrom, H. C., and W. A. Adcock (1950), A new iron carbide in hydrocarbon synthesis catalysts, *J. Am. Chem. Soc.*, *72*(2), 1042–1043.
Fang, C. M., M. A. van Huis, and H. W. Zandbergen (2009), Structural, electronic, and magnetic properties of iron carbide Fe_7C_3 phases from first-principles theory, *Phys. Rev. B*, *80*(22), 224108.
Fei, Y. W., and E. Brosh (2014), Experimental study and thermodynamic calculations of phase relations in the Fe-C system at high pressure, *Earth Planet. Sci. Lett.*, *408*, 155–162.
Fei, Y. W., A. Ricolleau, M. Frank, K. Mibe, G. Y. Shen, and V. Prakapenka (2007), Toward an internally consistent pressure scale, *Proc. Natl. Acad. Sci. U.S.A.*, *104*(22), 9182–9186.
Frost, D. J., C. Liebske, F. Langenhorst, C. A. McCammon, R. G. Tronnes, and D. C. Rubie (2004), Experimental evidence for the existence of iron-rich metal in the Earth's lower mantle, *Nature*, *428*(6981), 409–412.
Fruchart, R., and A. Rouault (1969), Twin crystals of orthorhombic isomorphous Cr_7C_3, Mn_7C_3, Fe_7C_3 Carbides, *Ann. Chim.*, *4*(3), 143–145.
Gao, L. L., et al. (2008), Pressure-induced magnetic transition and sound velocities of Fe_3C: Implications for carbon in the Earth's inner core, *Geophys. Res. Lett.*, *35*, L17306, doi:10.1029/2008GL034817.
Gorria, P., et al. (2009), Stress-induced large Curie temperature enhancement in $Fe_{64}Ni_{36}$ Invar alloy, *Phys. Rev. B*, *80*(6), 064421.
Guinan, M. W., and D. N. Beshers (1968), Pressure derivatives of the elastic constants of α-iron to 10 kbs, *J. Phys. Chem. Solids*, *29*(3), 541–549.
Herbstein, F. H., and J. A. Snyman (1964), Identification of Eckstrom-Adcock iron carbide as Fe_7C_3, *Inorg. Chem.*, *3*(6), 894–896.
Lin, J. F., V. V. Struzhkin, H. K. Mao, R. J. Hemley, P. Chow, M. Y. Hu, and J. Li (2004), Magnetic transition in compressed Fe_3C from X-ray emission spectroscopy, *Phys. Rev. B*, *70*(21), 212405.
Litasov, K. D., I. S. Sharygin, P. I. Dorogokupets, A. Shatskiy, P. N. Gavryushkin, T. S. Sokolova, E. Ohtani, J. Li, and K. Funakoshi (2013), Thermal equation of state and thermodynamic properties of iron carbide Fe_3C to 31 GPa and 1473 K, *J. Geophys. Res. Solid Earth*, *118*, 5274–5284, doi:10.1002/2013JB010270.
Litasov, K. D., S. V. Rashchenko, A. N. Shmakov, Y. N. Palyanov, and A. G. Sokol (2015), Thermal expansion of iron carbides, Fe_7C_3 and Fe_3C, at 297–911 K determined by in situ X-ray diffraction, *J. Alloys Compd.*, *628*, 102–106.
Liu, J., J. F. Lin, Z. Mao, and V. B. Prakapenka (2014), Thermal equation of state and spin transition of magnesiosiderite at high pressure and temperature, *Am. Mineral.*, *99*(1), 84–93.
Lord, O. T., M. J. Walter, R. Dasgupta, D. Walker, and S. M. Clark (2009), Melting in the Fe-C system to 70 GPa, *Earth Planet. Sci. Lett.*, *284*(1–2), 157–167.
Mao, H. K., J. Xu, and P. M. Bell (1986), Calibration of the ruby pressure gauge to 800-kbar under quasi-hydrostatic conditions, *J. Geophys. Res.*, *91*(B5), 4673–4676, doi:10.1029/JB091iB05p04673.
Mao, Z., J. F. Lin, J. Liu, and V. B. Prakapenka (2012), Thermal equation of state of lower-mantle ferropericlase across the spin crossover, *Geophys. Res. Lett.*, *39*, L02399, doi:10.1029/2011GL049915.
Mookherjee, M., Y. Nakajima, G. Steinle-Neumann, K. Glazyrin, X. A. Wu, L. Dubrovinsky, C. McCammon, and A. Chumakov (2011), High-pressure behavior of iron carbide (Fe_7C_3) at inner core conditions, *J. Geophys. Res.*, *116*, B04201, doi:10.1029/2010JB007819.
Moruzzi, V. L. (1990), High-spin and low-spin states in Invar and related alloys, *Phys. Rev. B*, *41*(10), 6939–6946.
Nakajima, Y., E. Takahashi, T. Suzuki, and K. Funakoshi (2009), "Carbon in the core" revisited, *Phys. Earth Planet Int.*, *174*, 202–211, doi:10.1016/J.Pepi.2008.05.014.
Nakajima, Y., E. Takahashi, N. Sata, Y. Nishihara, K. Hirose, K. Funakoshi, and Y. Ohishi (2011), Thermoelastic property and high-pressure stability of Fe_7C_3: Implication for iron-carbide in the Earth's core, *Am. Mineral.*, *96*(7), 1158–1165.
Nataf, L., F. Decremps, M. Gauthier, and B. Canny (2006), High-pressure structural study of $Fe_{64}Ni_{36}$ and $Fe_{72}Pt_{28}$ Invar alloys at low-temperature, *Phys. Rev. B*, *74*(18), 184422.
Ono, S., and K. Mibe (2010), Magnetic transition of iron carbide at high pressures, *Phys. Earth Planet. Int.*, *180*(1–2), 1–6.
Oomi, G., and N. Mori (1981), Pressure effect on the spontaneous volume magnetostriction of Fe-Ni and Fe-Pt Invar-alloys, *J. Phys. Soc. Jpn.*, *50*(9), 2924–2930.
Prescher, C., L. Dubrovinsky, C. McCammon, K. Glazyrin, Y. Nakajima, A. Kantor, M. Merlini, and M. Hanfland (2012), Structurally hidden magnetic transitions in Fe_3C at high pressures, *Phys. Rev. B*, *85*(14), 140402.
Prescher, C., et al. (2015), High Poisson's ratio of Earth's inner core explained by carbon alloying, *Nat. Geosci.*, *8*(3), 220–223.
Raza, Z., N. Shulumba, N. M. Caffrey, L. Dubrovinsky, and I. A. Abrikosov (2015), First-principles calculations of properties of orthorhombic iron carbide Fe_7C_3 at the Earth's core conditions, *Phys. Rev. B*, *91*(21), 214112.
Robie, R. A., B. S. Hemingway, and J. R. Fisher (1978), *Thermodynamic Properties of Minerals and Related Substances at 298.15 K and 1 Bar (10^5 Pascals) Pressure and at Higher Temperatures*, *U.S. Geol. Surv. Bull.*, pp. 456, AGU, Washington, D. C.
Rohrbach, A., and M. W. Schmidt (2011), Redox freezing and melting in the Earth's deep mantle resulting from carbon-iron redox coupling, *Nature*, *472*(7342), 209–212.
Rohrbach, A., C. Ballhaus, U. Golla-Schindler, P. Ulmer, V. S. Kamenetsky, and D. V. Kuzmin (2007), Metal saturation in the upper mantle, *Nature*, *449*(7161), 456–458.
Stagno, V., D. O. Ojwang, C. A. McCammon, and D. J. Frost (2013), The oxidation state of the mantle and the extraction of carbon from Earth's interior, *Nature*, *493*(7430), 84–88.
Tsuzuki, A., S. Sago, S. I. Hirano, and S. Naka (1984), High-temperature and pressure preparation and properties of iron carbides Fe_7C_3 and Fe_3C, *J. Mater. Sci.*, *19*(8), 2513–2518.
van Schilfgaarde, M., I. A. Abrikosov, and B. Johansson (1999), Origin of the Invar effect in iron-nickel alloys, *Nature*, *400*(6739), 46–49.
Vocadlo, L., J. Brodholt, D. P. Dobson, K. S. Knight, W. G. Marshall, G. D. Price, and I. G. Wood (2002), The effect of ferromagnetism on the equation of state of Fe_3C studied by first-principles calculations, *Earth Planet. Sci. Lett.*, *203*(1), 567–575.
Walker, D., R. Dasgupta, J. Li, and A. Buono (2013), Nonstoichiometry and growth of some Fe carbides, *Contrib. Mineral. Petrol.*, *166*(3), 935–957.
Walker, D., J. Li, B. Kalkan, and S. M. Clark (2015), Thermal, compositional, and compressional demagnetization of cementite, *Am. Mineral.*, *100*(11–12), 2610–2624.

Wang, F. M., and R. Ingalls (1998), Iron bcc-hcp transition: Local structure from X-ray-absorption fine structure, *Phys. Rev. B*, *57*(10), 5647–5654.
Weiss, R. J. (1963), Origin of Invar effect, *Proc. Phys. Soc.*, *82*(526), 281–288.
Winterrose, M. L., M. S. Lucas, A. F. Yue, I. Halevy, L. Mauger, J. A. Munoz, J. Z. Hu, M. Lerche, and B. Fultz (2009), Pressure-induced Invar behavior in Pd_3Fe, *Phys. Rev. Lett.*, *102*(23), 237202.
Wood, B. J. (1993), Carbon in the core, *Earth Planet. Sci. Lett.*, *117*(3–4), 593–607.
Wood, B. J., J. Li, and A. Shahar (2013), Carbon in the core: Its influence on the properties of core and mantle, *Rev. Mineral. Geochem.*, *75*, 231–250.
Xie, J. Y., N. X. Chen, J. Shen, L. D. Teng, and S. Seetharaman (2005), Atomistic study on the structure and thermodynamic properties of Cr_7C_3, Mn_7C_3, Fe_7C_3, *Acta Mater.*, *53*(9), 2727–2732.